A Spectral Parameterization of Mean-Flow Forcing due to Breaking Gravity Waves

M. J. ALEXANDER

Colorado Research Associates, Boulder, Colorado

T. J. DUNKERTON

NorthWest Research Associates, Bellevue, Washington

(Manuscript received 8 June 1998, in final form 18 March 1999)

ABSTRACT

A spectral parameterization of mean-flow forcing due to breaking gravity waves is described for application in the equations of motion in atmospheric models. The parameterization is based on linear theory and adheres closely to fundamental principles of conservation of wave action flux, linear stability, and wave–mean-flow interaction. Because the details of wave breakdown and nonlinear interactions are known to be very complex and are still poorly understood, only the simplest possible assumption is made: that the momentum fluxes carried by the waves are deposited locally and entirely at the altitude of linear wave breaking. This simple assumption allows a straightforward mapping of the momentum flux spectrum, input at a specified source altitude, into vertical profiles of mean-flow force. A coefficient of eddy diffusion can also be estimated. The parameterization can be used with any desired input spectrum of momentum flux. The results are sensitive to the details of this spectrum and also realistically sensitive to the background vertical shear and stability profiles. These sensitivities make the parameterization ideally suited for studying both the effects of gravity waves from unique sources like topography and convection as well as generalized broad input spectra. Existing constraints on input parameters are also summarized from the available observations. With these constraints, the parameterization generates realistic variations in gravity-wave-driven, mean-flow forcing.

1. Introduction

Gravity waves are mesoscale phenomena that have important global effects on the circulation, temperature structure, chemistry, and composition of the atmosphere. Atmospheric gravity waves have typical horizontal wavelengths of tens to thousands of kilometers and periods ranging from minutes to many hours. Observations show these waves to be highly variable in their properties, but they are ubiquitous features in high-resolution data. Their small scales and short periods make their global properties difficult to quantify in currently available meteorological data and difficult to resolve in most global models.

Gravity waves carry momentum and energy vertically in the atmosphere leading to important forcing terms in the momentum and energy budget equations in global models. These forcing terms are accounted for via parameterizations of gravity wave effects that use the information on the larger-scale wind and stability fields. Lindzen (1981) developed a successful parameterization of gravity wave effects that has been widely applied in atmospheric models. Important modifications were made by Holton (1982) and Lindzen (1985), and subsequent application of these basic ideas to the effects of waves forced by flow over topography were developed and applied in global models by Palmer et al. (1986) and McFarlane (1987). These Lindzen-type parameterizations are based on the fundamental physical principles of wave stability and momentum flux conservation for a monochromatic gravity wave. The use of ''monochromatic'' here refers to a single ground-relative phase speed and horizontal wavenumber combination. The dissipation of the wave as a function of height is based on the concept of ''saturation'' (Fritts 1984; Dunkerton 1989) and allows the wave to continue propagating above the level of linear instability onset by assuming enough dissipation for the wave to remain stable. Parameterizations of this type are still in wide use today (e.g., Keihl et al. 1996; Norton and Thuburn 1996).

The importance of realistically describing the effects of the broad spectrum of gravity waves present in the atmosphere is widely recognized and has led to the proposal of several spectral parameterization schemes in recent years (Fritts and VanZandt 1993; Fritts and Lu 1993; Medvedev and Klaassen 1995; Hines 1997). The

Corresponding author address: Dr. M. Joan Alexander, Colorado Research Associates, 3380 Mitchell Lane, Boulder, CO 80301.
E-mail: alexand@colorado-research.com

first attempt at a spectral parameterization was described in Lindzen and Holton (1968, hereafter LH68) and applied to the problem of forcing the quasi-biennial oscillation (QBO) in the tropical stratosphere. This parameterization assumes that the waves deposit all the momentum they carry at their critical level: namely, where the phase speed of the wave equals the background wind speed in the direction of wave propagation. In the case of a monochromatic wave, this would lead to a delta function of forcing in the vertical; but when a full spectrum of waves is considered, it leads to a simple formula for mapping the spectrum of momentum flux carried by the waves onto the profile of background winds as a function of height. This approach was largely abandoned for its original purpose of explaining the QBO in favor of the proposed planetary-scale wave forcing mechanism of Holton and Lindzen (1972), but was shown to be a reasonable, although oversimplified, model of gravity wave mean-flow forcing in the lower stratosphere by Dunkerton (1997) and Alexander and Holton (1997). The waves cannot propagate to the theoretical critical level without suffering severe dissipation, but the typically low amplitudes in the stratosphere result in this dissipation occuring near enough to the critical level for the LH68 assumption to be reasonable. In the mesosphere, the LH68 parameterization would fail to describe the drag force responsible for reversing the radiative equilibrium summer-to-winter temperature gradient and the zonal-mean meridional circulation inferred from observed temperatures and chemical composition because wave dissipation must occur far from critical levels. LH68 also cannot describe mountain wave drag on the midlatitude winter lower stratosphere circulation.

The parameterization we propose here is a hybrid and extension of the ideas and mathematics in Lindzen (1981) and Lindzen and Holton (1968). We use the Lindzen (1981) breaking criterion, then deposit the wave momentum flux locally and totally at the breaking level in a manner analogous to Lindzen and Holton's (1968) assumption. We include the additional physical process of total internal wave reflection at high frequencies.

A fundamental concept that underlies our spectral approach is that wave forcing is intermittent. We base our assumption of intermittency on the combined constraints of observations and models described in the next section. A spectrum of momentum flux must be input to the parameterization as a function of phase speed (c). This spectrum is meant to describe a collection of wave packets of finite size in both horizontal area and in time. The intermittency describes the fraction of time and space that each wave packet is forced. It would be unity if the forcing were continuous. The concept of intermittency lies behind the use of an ''efficiency factor'' that is generally applied in Lindzen-type parameterizations, and here is formally related to observable properties of the gravity wave spectrum. If the wave phase speed spectrum is defined coarsely, then the parameterization resembles Lindzen-type parameterizations that use a small number of phase speeds to describe the gravity wave spectrum. Thus, at coarse resolution the difference between this parameterization and various Lindzen-type applications is in the manner by which the momentum flux is distributed with height between the breaking level and critical level. If the spectrum is instead defined with fine phase speed resolution, then each band Δc defines a smaller fraction of the spectrum and naturally is accompanied by a smaller intermittency per band. Put simply, one can imagine that some type of gravity wave might always be forced somewhere within a model grid box, but a wave with very specific properties might only occur very infrequently. So it is the intermittency per band that changes with Δc in our formulation, not the amplitudes of the waves. The latter determine the breaking levels, are specified separately, and can be constrained by observations of wave events.

Our approach uses linear monochromatic theory to describe propagation and instability onset of individual small bands of the spectrum and takes this assumption of intermittency to an extreme. However, dispersion of wave packets can be observed in wave propagation models (Alexander 1996; Prusa et al. 1996), and a high degree of dispersion is implied by the nearly monochromatic gravity wave events observed near the mesopause (Swenson and Espy 1995; Taylor et al. 1995). These suggest that our approach may be considered an oversimplified but not unreasonable approximation to gravity wave behavior.

Our parameterization treats each wave in the spectrum independently, neglecting wave–wave interactions. The validity of this assumption is questionable for waves with slow vertical group velocities (short vertical wavelength, long period gravity waves) (Broutman et al. 1997; Eckermann 1997). These waves populate the high vertical wavenumber (m) end of the energy spectrum. Observed gravity wave spectra at short vertical wavelengths ($O \sim 1$ km or less) typically display a characteristic m^{-3} shape called the ''tail'' of the the m spectrum. Wave theory suggests that these waves are likely suffering dissipation because the amplitudes are close to limits imposed by instability theory, and the decreasing energy with increasing m has been related to various instability and dissipation mechanisms (Dewan and Good 1986; Smith et al. 1987; Fritts 1989; Hines 1991; Zhu 1994). This high-m tail part of the spectrum is also more likely to be affected by interactions with other waves (Hines 1991; Broutman et al. 1997; Eckermann 1997). Waves at the other end of the spectrum, those with long vertical wavelengths and high intrinsic frequencies, will have fast vertical group velocities. These waves are much better described by linear theory, are generally observed with amplitudes substantially below instability limits, and are much less likely to be affected by wave–wave interactions.

Our parameterization approach treats these faster waves, which likely carry a large fraction of the mo-

mentum flux (Fritts and Vincent 1987), with linear theory. Wave refraction to smaller vertical wavelengths and lower intrinsic frequencies occurs in this approach through interaction with a vertically varying background atmosphere. This part of the problem is given careful treatment with linear theory, but when the wave is refracted into the tail of the spectrum and reaches a point where it is unstable, it is simply removed from the spectrum for mathematical convenience. We therefore do not treat the details of dissipation realistically, but by choosing a smooth function of momentum flux versus phase speed as input, realistically smooth profiles of mean-flow forcing are still achieved. The background flow must be slowly varying according to our assumptions, but could be anything from low phase speed planetary-scale waves to a simple seasonally varying zonal-mean state. We use the onset of convective instability derived from linear theory as the dissipation criterion, but other criteria could be used in future applications of the parameterization if our knowledge of the details of wave dissipation mechanisms improves.

Our assumption that gravity waves occur only intermittently is also most valid for this fast vertical group velocity part of the spectrum. Our parameterization thus emphasizes the importance of the long vertical wavelength, short intrinsic period gravity waves outside the tail of the spectrum to the momentum budget of the problem. It also assumes that the short vertical wavelength, long period waves will have slow enough vertical group velocities that they are close to the altitude where they will be dissipated. Then the approximation of removing them from the budget is reasonable.

We first review the constraints on wave amplitudes and total momentum flux that support intermittency, the monochromatic linear theory for gravity wave instability and wave–mean-flow interaction, and the background ideas of Lindzen (1981), Holton (1982), and Lindzen and Holton (1968) in section 2. The parameterization, as described in section 3, is presented as a tool for numerical models seeking to include the effects of a spectrum of gravity waves on the background atmosphere. Section 4 illustrates the kinds of results that can be obtained. We end with some discussion in section 5.

2. Background

We seek to parameterize the vertical profile of mean-flow forcing due to a spectrum of wave momentum flux whose source is specified at height z_0 somewhere below. This forcing would be applied in the horizontal momentum balance equations in a model. For the zonal-mean flow, for example,

$$\frac{d\overline{u}}{dt} - f\overline{v} = \overline{X}, \tag{1}$$

where $\overline{u}$, $\overline{v}$ are the zonal mean zonal and meridional wind, f the Coriolis parameter, and $\overline{X}$ the zonal-mean zonal force due to gravity wave dissipation (Andrews et al. 1987). The wave propagation is treated as one-dimensional, neglecting horizontal variations and wave-packet distortions. Azimuthal spreading that would be associated with waves emanating from a point source (e.g., Dewan et al. 1998) is also neglected. These assumptions will be most applicable to global models with coarse horizontal resolution.

Our approach to parameterizing $\overline{X}$ is based on an underlying assumption that the momentum transport responsible for the gravity wave dissipation occurs intermittently in discrete events, but that the net effect of interest to global modelers is a time- and space-averaged envelope describing those events.

a. Constraints on gravity wave source amplitudes and total momentum fluxes

We base our assumption of intermittency on the combined constraints of observations and models. Observations of momentum fluxes just above the tropopause carried by gravity waves and linked to specific sources like topography (Palmer et al. 1986; Fritts et al. 1990; Prichard et al. 1995; Sato 1990) and convection (Pfister et al. 1993; Alexander and Pfister 1995; Sato 1993) often show large values during wave ''events'' or ''active times.'' These are commonly reported as $\overline{u'w'}$ in meters squared per second squared, but here we multiply by density in order to compare observations at different altitudes. Over topography, the magnitudes of these event amplitudes are in the range ~0.03–0.5 Pa. Above active convection, 0.03–0.15 Pa have been reported. Conversely, long-term averages of wave momentum fluxes or fluxes measured during ''quiet times'' are observed to be much smaller. Over mountainous terrain, values $\leq$0.06 Pa have been reported with values ~0.01 Pa most common (Prichard and Thomas 1993; Fritts et al. 1990; Sato 1994; Sato et al. 1997; Murayama et al. 1994) and at other locations 0.001–0.02 Pa (Sato and Dunkerton 1997; Chang et al. 1997). Since nonevents are rarely reported, a better estimate of the long-term, global-scale fluxes carried by gravity waves come from model studies that estimate the gravity wave momentum fluxes indirectly using constraints on the mean-flow forcing due to gravity waves in the middle atmosphere (Fritts 1989; Alexander and Rosenlof 1996; Ray et al. 1998; Dunkerton 1997). At extratropical latitudes, estimated average fluxes required to drive the mean meridional residual circulation are 0.003–0.006 Pa (Alexander and Rosenlof 1996). At tropical latitudes, an estimated momentum flux of 0.002–0.003 Pa is needed to drive both the QBO (Dunkerton 1997) and stratopause semiannual oscillation (Ray et al. 1998) winds. These are roughly 5–100 times smaller than the fluxes observed directly over wave sources, supporting our assumptions of highly intermittent wave sources. Intermittency is also supported by wavelet analyses of observations (Sato and Yamada 1994) whereas traditional Fourier analysis inherently averages away much of the

information about intermittency that may be available. Other gravity wave–generation mechanisms, such as geostrophic adjustment, are likely associated with baroclinic systems (O'Sullivan and Dunkerton 1995) and weather fronts (Reeder and Griffiths 1996), and these sources are also expected to be intermittent.

b. Linear wave theory for slowly varying background flows

Linear wave theory predicts that in the absence of dissipation a wave will propagate, conserving wave action flux through variable background winds (Lighthill 1978). If these background winds are presumed to be horizontally uniform with only vertical shear, then both the vertical components of the wave action flux F_A and the pseudomomentum flux F_P are conserved:

$$F_A = \overline{\rho}\frac{E}{\omega}c_{gz} = F_P/k = \text{constant}. \tag{2}$$

Here $\overline{\rho}$ is the background density that decreases exponentially with height z, E is the total wave energy per unit mass, ω is the intrinsic frequency, c_{gz} is the vertical group velocity, and the horizontal wavenumber k is a constant under these conditions. The pseudomomentum flux can be divided into zonal and meridional components ($F_{P\lambda}$, $F_{P\phi}$) according to the direction of wave propagation. The force $\tilde{X}$ on the local background flow due to gravity wave dissipation is associated with the vertical gradient of the pseudomomentum flux. For the zonal component,

$$\tilde{X} = \frac{-1}{\overline{\rho}}\frac{\partial}{\partial z}(F_{P\lambda}). \tag{3}$$

An equation of this form applies to both horizontal coordinates (e.g., longitude λ and latitude ϕ). For waves propagating westward relative to the mean flow, $F_{P\lambda}$ is negative, while it is positive for waves propagating eastward. The pseudomomentum flux is related to the Reynold's stress and momentum flux (Fritts and Vincent 1987),

$$F_{P\lambda} = \overline{\rho}\,\overline{u'w'}(1 - f^2/\omega^2), \tag{4}$$

where $\overline{u'w'}$ represents an average over a wavelength or period of the horizontal (u') and vertical (w') wind perturbations associated with the wave. The pseudomomentum flux in (4) is the negative of the vertical component of the Eliassen–Palm flux for gravity waves (Andrews et al. 1987). The momentum flux $\overline{\rho}\,\overline{u'w'}$ is the quantity that can be determined from many observation techniques. The intrinsic frequency ω is generally difficult to determine from observations. Equation (4) shows that the momentum flux is equivalent to the pseudomomentum flux for higher-frequency gravity waves ($\omega^2 \gg f^2$).

If there is intermittency in the wave forcing and gravity waves travel in packets of finite size, the zonal-mean force or force applied on some larger scale X must include a fractional coverage ε of the breaking waves in the space and time over which the force is to be applied:

$$X = \frac{-\varepsilon}{\overline{\rho}}\frac{\partial}{\partial z}(F_{P\lambda}). \tag{5}$$

We call ε the intermittency. An example of how ε can be computed for convectively generated gravity waves in a numerical model appears in Alexander (1996). From most currently available observations, ε cannot be determined, except perhaps from continuously operating ST radars (e.g., Sato 1992; Sato et al. 1997). Until more data on wave intermittency in the lower stratosphere are available, ε is a loosely constrained, free parameter in these calculations. It may vary on a wide range of timescales, may vary with geography, and may be a function of the wave packet properties as well, for example, $\varepsilon(\lambda, \phi, t, \omega, k)$. If treated as a constant, it can be estimated indirectly by comparing amplitudes in wave events $\overline{u'w}$ to estimates of the seasonally varying forcing in the middle atmosphere (Alexander and Rosenlof 1996) described in the beginning of this section.

c. Lindzen-type monochromatic parameterizations

Lindzen (1981, hereafter L81) described a parameterization for the force due to a monochromatic wave based on the fundamental ideas of linear wave theory, instability, and conservation of momentum flux. He assumed conservative propagation of the wave up to the level where the wave was convectively unstable. The level of instability, called the breaking level z_b, can be defined as that height where the source flux F_{P0} matches the criterion

$$F_{P0} = \left[\frac{\overline{\rho}(z)k}{2N(z)}(c - \overline{u}(z))^3\right]_{z=z_b}. \tag{6}$$

Here, c is the phase speed and N is the buoyancy frequency. This condition is derived assuming the waves are hydrostatic, nonrotating, and breaking at vertical wavelengths $\lambda_z \ll 4\pi H$, where H is the density-scale height. Below z_b, F_{P0} must be smaller than the right-hand side of (6). L81 assumed that the gravity wave force would be roughly constant with height between the breaking level z_b and the critical level z_c. Holton (1982) derived a vertical profile for this force by assuming that the wave is saturated, transferring enough momentum and energy to the background atmosphere to remain stable. This leads to a forcing profile above z_b with the form

$$X = \frac{-\varepsilon k}{2N}(\overline{u} - c)^3\left(\frac{1}{H} - \frac{3d\overline{u}/dz}{\overline{u} - c}\right) \quad \text{for } z_b < z < z_c. \tag{7}$$

The force X estimated from (7) is generally multiplied by a scaling factor, or "efficiency factor," of ~0.1 that can be thought of as describing the intermittency in the

wave forcing (Holton 1982). Multiple breaking levels can be accomodated with modifications described in McFarlane (1987) and Kiehl et al. (1996). In global models, the Lindzen parameterization is applied with some discrete set of phase speeds (e.g., Garcia and Solomon 1985; Rind et al. 1988; Jackson and Gray 1994). The breaking level is determined for each phase speed $z_b(c)$, and the force profile computed with (7). Unless a sufficiently large set of phase speeds is selected, the parameterization predicts sudden jumps in the forcing at the breaking levels $z_b(c)$, so some form of gradual onset of the force may be included to facilitate its inclusion in numerical models. This has been justified as either representing turbulence generated by nonbreaking waves (Lindzen 1981) or as associated with breaking of the broader spectrum of waves not treated in the monochromatic formula (Holton 1982).

Holton (1982) also derived the relationship between the eddy diffusion coefficient D and X for this parameterization:

$$D = \frac{(c - \overline{u})}{N^2} X. \tag{8}$$

This coefficient has been applied to describe vertical diffusive mixing terms in the momentum and energy equations (e.g., Holton 1982). There is, however, still considerable uncertainty in how the energy in the wave breakdown process should be partitioned to vertical mixing (Fritts and Dunkerton 1985; Coy and Fritts 1988; McIntyre 1989; Lelong and Dunkerton 1998a,b). An energy dissipation rate, $(c - \overline{u})X$, is also implied under our assumptions (e.g., Fritts and VanZandt 1993).

d. Lindzen and Holton (1968) parameterization

Lindzen and Holton (1968) parameterized the effects of breaking gravity waves in the QBO by assuming a spectrum of phase speeds c and by assuming that breaking occurs at critical levels. The critical level z_c is that level where the phase speed equals the mean wind speed in the direction of wave propagation, or for zonally propagating waves $c = \overline{u}(z_c)$. The waves were assumed to propagate conservatively below z_c but to deposit all the momentum they carry at z_c. For a monochromatic gravity wave, this would lead to a step function in the momentum flux profile and a Dirac delta function in the forcing at height z_c. In the case of a spectrum of wave phase speeds defined at resolution Δc, these assumptions lead to a simple mapping of the source momentum flux spectrum per unit phase speed $\hat{f}(c)$ onto the background wind profile:

$$\hat{f}(c) \mapsto \hat{f}[\overline{u}(z_c)], \tag{9}$$

taking care to map the flux at c only once to the first z_c above z_0. The wave-driven mean-flow force can then be shown to be

$$X = |\hat{f}(\overline{u})| \frac{\overline{\rho}_0}{\overline{\rho}} \frac{d\overline{u}}{dz}, \tag{10}$$

where $\overline{\rho}_0$ is the density at the source level z_0. The source flux $\hat{f}(c)$ can be related to the previous terminology for monochromatic pseudomomentum flux via

$$\hat{f}(c) = \frac{\varepsilon F_{P0}(c)}{\overline{\rho}_0 \Delta c}. \tag{11}$$

Equation (10) predicts that the wave-driven force will always have the same sign as the background shear and the force will be zero if the shear goes to zero. The force in (10) leads to descent of an existing shear zone, but it cannot initiate one. Equation (10) also cannot describe the inferred gravity wave–driven drag force in the mesosphere nor the mountain wave drag in the lower stratosphere above the winter midlatitude jet. Both of these phenomena require wave breaking and momentum deposition well below wave critical levels.

Dunkerton (1997) compared the LH68 result to a detailed spectral line-by-line calculation of the forcing in typical QBO-like shears in the lower stratosphere. Alexander and Holton (1997) compared the results of the LH68 parameterization to the mean-flow forcing in a two-dimensional nonlinear numerical model of the lower stratosphere. Their results show that the LH68 parameterization results are similar to those seen in the nonlinear model, but that the momentum carried by the waves deposited a finite distance below the critical level. This result is expected because most wave instability and dissipation mechanisms become more likely as a wave approaches its critical level from below.

3. The spectral parameterization

The parameterization we propose here combines ideas from both the LH68 and L81 parameterizations. The spectrum is treated as a collection of monochromatic wave packets. Each packet is assumed to propagate vertically through varying background wind and stability conserving pseudomomentum flux below the breaking level. At the breaking levels z_b, the waves are assumed to deposit all the momentum they carry. No saturation condition is applied above the breaking level. This assumption sidesteps the details of the complex wave breakdown process (Fritts and Dunkerton 1985; Dunkerton 1989; Andreassen et al. 1994; Fritts et al. 1994; Lelong and Dunkerton 1998a,b) while permitting a simple mapping of the gravity wave pseudomomentum flux in the vertical. This simplifying assumption implies that the wave-induced force per unit phase speed is proportional to a Dirac delta function peaking at z_b, $\delta(z - z_b)$, rather than $\delta(z - z_c)$ as in LH68, leading to a modified version of (10) with $(\partial z_b/\partial c)^{-1}$ in place of $(\partial \overline{u}/\partial z)$, as shown by Dunkerton (1997). In the limit Δz, $\Delta c \to 0$ the force can become singular, when $\partial z_b/\partial c = 0$. This could occur if several waves in the spectrum break at the same altitude, but the problem is avoided in finite

grid box models where $|\Delta z| > 0$. Here we develop a numerical solution embodying these same physical concepts.

Let $F_{P0}(c)$ represent a discrete set of waves with phase speeds $\{c_i\}$ specified at resolution Δc carrying momentum flux $\{F_{P0}(c_i)\}$. Let F_S represent the total momentum flux in the gravity wave spectrum at some height z above the source level z_0:

$$F_S(z) = \sum_i F_{P0}(c_i), \quad \text{for } z_b(c_i) > z. \tag{12}$$

The monochromatic mean-flow force given by (5) can be extended to a spectrum of waves by totaling contributions from all the elements of the spectrum,

$$X(z) = \frac{-\varepsilon}{\overline{\rho}(z)} \frac{\partial}{\partial z}[F_S(z)]. \tag{13}$$

With our assumption of total momentum dissipation at the breaking level, the gradient in the flux

$$\frac{\partial}{\partial z}(F_S) = -\sum_j (F_{P0})_j/\Delta z, \quad \text{for } (z - \Delta z) < z_b(c_j) \le z, \tag{14}$$

where the sum over index j represents a sum of momentum fluxes for waves in the spectrum that are breaking in a vertical grid interval Δz and $(F_{P0})_j = F_{P0}(c_j)$. Let z_h represent a half-interval step $z - \Delta z/2$. Then the parameterized force is

$$X(z_h) = \frac{\varepsilon}{\overline{\rho}(z_h)\Delta z} \sum_j (F_{P0})_j \quad \text{for } (z - \Delta z) < z_b(c_j) \le z, \tag{15}$$

summing over the j waves that break in the height interval Δz. The factor ε is the intermittency, assumed constant here, but that could easily be allowed a phase speed dependence by moving ε_j inside the sum in (15). By analogy with (8),

$$D(z_h) = \frac{\varepsilon}{\overline{\rho}(z_h)N^2(z_h)\Delta z} \sum_j [c_j - \overline{u}(z_h)](F_{P0})_j \quad \text{for } (z - \Delta z) < z_b(c_j) \le z. \tag{16}$$

To find the relationship between the breaking levels z_b and the amplitudes in the source spectrum F_{P0}, the L81 condition (6) is used. Nonhydrostatic and rotation effects excluded in the derivation of (6) can be included in the determination of the breaking level at the cost of greater complexity, but the effect on the resulting forcing estimates will be shown to be rather small. Neglecting rotation also means the pseudomomentum flux (2) is equivalent to the vertical flux of horizontal momentum $\overline{\rho}\,\overline{u'w'}$, which can be determined by observations. Hereafter we will refer to F_P as simply momentum flux. The schematic diagrams in Fig. 1 illustrate the assumptions employed in LH68, Lindzen-type, and the present parameterization considering only a single monochromatic wave.

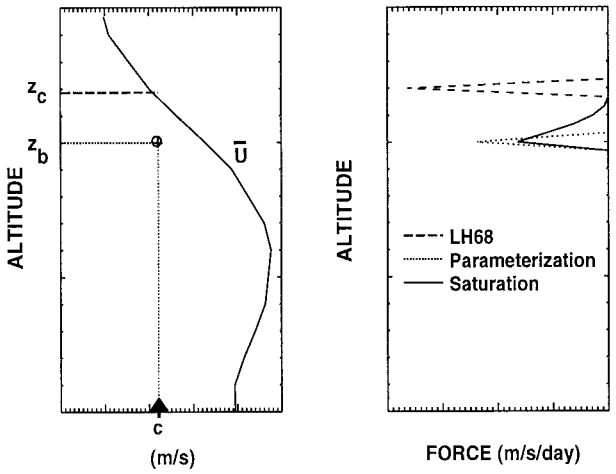

FIG. 1. Schematic diagram showing the relationships between (a) breaking z_b and critical z_c levels for a monochromatic wave with phase speed c propagating through mean wind profile U, and (b) the wave-driven force predicted with the three gravity wave parameterization assumptions described in sections 2 and 3.

Although the hydrostatic approximation is appropriate for determining the breaking level where intrinsic frequencies are fairly low, the parameterization includes the important nonhydrostatic process of total internal reflection of gravity waves that occurs when waves are Doppler shifted to high intrinsic frequencies. Total reflection severely limits propagation of the shorter horizontal wavelength waves (<100 km) into the upper stratosphere and mesosphere during solstice seasons. It will be explained in more detail later in this section.

The parameterization can be applied in any azimuthal direction. The examples developed in section 4 show results for two azimuths (east and west) and the zonal gravity wave–driven force based on zonal-mean wind and stability fields.

a. The source spectrum

To begin, a discrete spectrum of wave momentum flux versus phase speed must be specified at the source level z_0. We will work here primarily with the class of functions

$$B_0(c) \equiv \frac{F_{P0}(c)}{\overline{\rho}_0} = \text{sgn}(\hat{c})B_m \exp\left[-\left(\frac{c - c_0}{c_w}\right)^2 \ln 2\right]. \tag{17}$$

Here c is the ground-relative phase speed; c_0 is the phase speed with maximum flux magnitude B_m; c_w is the half-width at half-maximum of the Gaussian; and $\hat{c}$ is the intrinsic phase speed at z_0,

$$\hat{c} = c - \overline{u}_0, \tag{18}$$

where $\overline{u}_0 = \overline{u}(z_0)$. As previously noted, $F_{P0}(c)$ is a discrete set of momentum flux amplitudes at the source level composing a spectrum that will be used to determine breaking levels. Here B_m and $B_0(c)$ (units of m^2

s^{-2}) can be constrained with observations of $\overline{u'w'}$ and $\overline{v'w'}$ in local wave events. The amplitudes during active times, contained in $B_0(c)$, together with the mean-flow profile largely determine at what level the waves will break.

The total momentum flux in the spectrum is specified with a separate parameter F_{S0}, which can be constrained with long-term averages of observed $\overline{u'w'}$ and $\overline{v'w'}$. Such long-term averages give a measure of the average flux crossing the surface at height z_0 including both wave events as well as quiet times. If B_m, F_{S0}, and c_w are all input to the model, this implies an average intermittency factor, ε, via

$$\varepsilon = \frac{F_{S0}\Delta c}{\overline{\rho}_0 \sum_c |B_0(c)|\Delta c}. \tag{19}$$

Written this way, Eq. (19) states that the intermittency ε is proportional to the ratio of the total time average momentum flux F_{S0} to the integral of the momentum flux amplitude spectrum. The dependence of ε on Δc is also explicit here. For the example amplitude spectrum given by Eq. (17), the intermittency $\varepsilon = 2(\ln 2/\pi)^{1/2}[F_{S0}/(\overline{\rho}_0 B_m)](\Delta c/c_w)$ if the range of phase speeds is large enough to approximate the sum in (19) as an integral from $\pm\infty$.

Parameters ε and c_w are the least well constrained by observations. Here we will choose to specify B_m, F_{S0}, and c_w to define the source spectrum. A value of k or set of k values must also be chosen and the flux F_{S0} partitioned among them. These together will imply an ε if it is treated as a constant, but note that ε could instead be a specified parameter, and it could vary as $\varepsilon(\lambda, \phi, t, c, k)$ within the formulation described here. The value of ε will in general be proportional to the phase speed resolution Δc specified in the source spectrum since a wave with properties described by a narrow band width Δc should occur much less frequently than one within a broad Δc band. Note that the parameterization can accomodate any arbitrarily shaped source spectrum, although source spectra that contain sharp peaks of momentum flux will lead to peaks in the vertical profile of forcing at the breaking level that may be unrealistically narrow if the ideas of saturation are more realistic than our assumption of shallow dissipation within a grid interval.

b. *Mapping F_{P0} into the vertical profile of mean-flow forcing and eddy diffusion*

Instead of computing breaking levels and forcing profiles for each member of the phase speed spectrum (as in Lindzen-type parameterizations), we instead ask which phase speeds are unstable at each model grid level. The answer gives the portion of the momentum flux in the source spectrum that is to be deposited at each level that leads to a simple measure of the momentum flux convergence in each altitude interval.

The following procedures describe the numerical details of the momentum budget. Let z_n be the set of model grid points equally spaced at resolution Δz. At the specified source level $z_n = z_0$, we check whether the magnitude of the intrinsic frequency,

$$|\omega| = k|c - \overline{u}_0|, \tag{20}$$

is less than the reflection frequency

$$\omega_r = \left(\frac{N^2k^2}{k^2 + \alpha^2}\right)^{1/2}. \tag{21}$$

Waves with $|\omega| \geq \omega_r$ would have undergone total internal reflection somewhere below and are eliminated from the spectrum. This reflection frequency neglects acoustic gravity wave properties, but these are minor corrections (Marks and Eckermann 1995). The term $\alpha = 1/(2H)$ is an important correction term at the high intrinsic frequencies where total internal reflection occurs [see Fig. 1 of Marks and Eckermann (1995)]. Next, we check the remainder of the spectrum for stability with the condition

$$Q_0(c) = \frac{2N(z_0)B_0(c)}{k(c - \overline{u}_0)^3} < 1. \tag{22}$$

Any waves with $Q_0 \geq 1$ are not stable at the source level. These waves are also removed from the spectrum. The remaining waves that are propagating and stable define the input momentum flux spectrum at the source level z_0.

Now working upward in altitude, we test the remaining waves at level z_n for total internal reflection by computing

$$|\omega| = k|c - \overline{u}(z_n)|, \tag{23}$$

and ω_r with (21) using values at z_n. Waves for which $|\omega| \geq \omega_r$ are reflected and eliminated. Next we compute

$$Q_n(c) = \frac{\overline{\rho}_0}{\overline{\rho}(z_n)} \frac{2N(z_n)B_0(c)}{k[c - \overline{u}(z_n)]^3}. \tag{24}$$

Breaking waves are those for which $Q_n \geq 1$. This portion of the spectrum was dissipated between levels z_{n-1} and z_n. Summing over any waves (j) that have not been reflected, that had not previously broken at lower levels, and for which $Q_n \geq 1$ yields

$$X(z_{n-1/2}) = \frac{\varepsilon}{\overline{\rho}(z_{n-1/2})\Delta z} \sum_j (F_{P0})_j \quad \text{for } (z_n - \Delta z) < z_b(c_j) \leq z_n \tag{25}$$

$$D(z_{n-1/2}) = \frac{\varepsilon \sum_j (c_j - \overline{u}(z_{n-1/2}))(F_{P0})_j}{\overline{\rho}(z_{n-1/2})N^2(z_{n-1/2})\Delta z} \quad \text{for } (z_n - \Delta z) < z_b(c_j) \leq z_n, \tag{26}$$

where $z_{n-1/2} = z_n - \Delta z/2$. These are the mean-flow forcing and eddy diffusion coefficient estimates due to

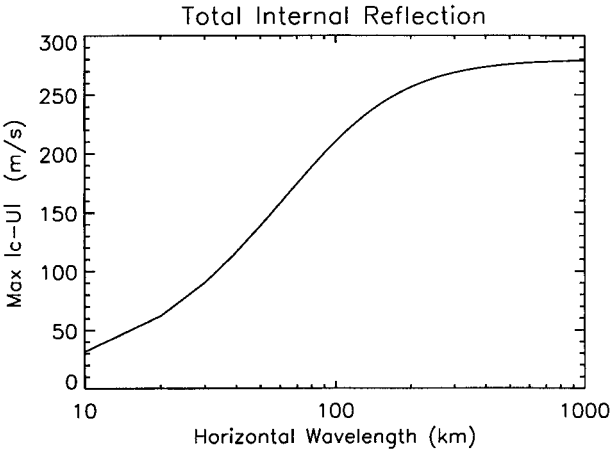

FIG. 2. Maximum intrinsic phase speed that can propagate as a gravity wave as a function of horizontal wavelength. A scale height of 7 km and buoyancy frequency of 0.02 s^{-1} have been assumed.

waves that broke between levels z_{n-1} and z_n. It is therefore appropriate to average these values with those stored at the previous level, which represented the force and diffusion at level $z_{n-3/2}$. So we back-substitute:

$$X(z_{n-1}) = \frac{1}{2}[X(z_{n-3/2}) + X(z_{n-1/2})] \quad (27)$$

$$D(z_{n-1}) = \frac{1}{2}[D(z_{n-3/2}) + D(z_{n-1/2})]. \quad (28)$$

Note that some source shapes are amenable to analytical integration over finite phase speed limits. For these functions, analytical formulas may replace the numerical integrations given here for potential time savings. We anticipate that the value of a parameterization that can treat any input spectral shape will override such computing-time benefits in the long run.

c. *Horizontal wavelengths and total internal reflection*

The effects of total internal reflection of waves Doppler-shifted to high intrinsic frequency have not been treated in previous parameterization schemes employed to date. Marks and Eckermann (1995) developed the criterion for reflection of waves propagating in an atmosphere with variable winds, stability, and finite scale height H. Their criterion, simplified to two-dimensional wave propagation, is employed in (21). This is the condition used in the linear model with saturation by Alexander (1998). In Alexander (1996) and Warner and McIntyre (1996) a similar condition was used, but the effects of the finite scale height were neglected so that $\alpha^2 \cong 0$, and the reflection frequency ω_r was equal to the buoyancy frequency N in these models. Marks and Eckermann (1995) describe differences between these criteria as a function of horizontal wavenumber k. Figure 2 shows the maximum intrinsic phase speed (ω_r/k) allowed before reflection occurs as a function of horizontal wavelength. Only low intrinsic phase speeds less than 30 m s^{-1} are allowed for horizontal wavelengths as short as 10 km. It is these smaller-scale waves <100 km that are most seriously affected by reflection.

Figures 3, 4, and 5 compare the results of the parameterization, with and without the process of total internal reflection, to the linear model with saturation used by Alexander (1998). The linear model is similar to Lindzen-type parameterizations, but it includes rotation, nonhydrostatic, and reflection effects. The same spectrum of waves is applied in both the linear model and the parameterization. Background winds and stability are taken from CIRA (COSPAR International Reference Atmosphere, Fleming et al. 1990) for January at 40°N latitude. The input parameters for these examples are listed in Table 1 (''broad''). Figure 3 assumes a single horizontal wavelength of 10 km and a spectrum of phase speeds c. Neglecting reflection (dashed line) leads to a prediction of a large force of ~ -500 m s^{-1} day^{-1} near the mesopause (Fig. 3a). The force at these altitudes is exactly zero when reflection is included (solid line in Figs. 3a,c) because all westward-propagating waves have been reflected at altitudes in the stratosphere below (Fig. 3b). Figure 3c shows the force in the stratosphere on an expanded scale. Reflection also limits vertical propagation of high positive phase speeds and reduces the force predicted in the upper stratosphere for this case.

Figure 4 shows the same calculation assuming a 100-km horizontal wavelength. At this longer horizontal wavelength, total internal reflection is no longer important for the range of wind speeds considered here. The parameterized force (solid lines in Figs. 4a,c) is similar in magnitude and vertical structure to the linear model with saturation (dotted lines). The differences in the mesosphere (Fig. 4a) are mainly attributable to the difference between the saturation assumption and the parameterized breaking assumption. Saturation leads to deposition of more momentum at higher altitudes where the density is lower. This leads to a higher and larger peak in the force according to (3). In the stratosphere (Fig. 4c), the differences between the parameterization and the linear model are again small.

For even longer wavelength waves, $k = 2\pi/(1000$ km) shown in Fig. 5, breaking occurs at lower altitudes than for waves with the same source amplitudes but larger k [Eq. (6)]. Now waves break far below their critical levels (Fig. 5b) and the differences between the parameterized dissipation and the saturation condition are even more apparent in the mesosphere. Note that breaking levels for all the waves in Figs. 3–5 are very similar in the parameterization and the linear model (cf. panels b and d in each). This result shows that the hydrostatic approximation and the neglect of rotation in the determination of the breaking levels have only minor effects on the results, although models wishing to treat large-amplitude, long-wavelength gravity waves may

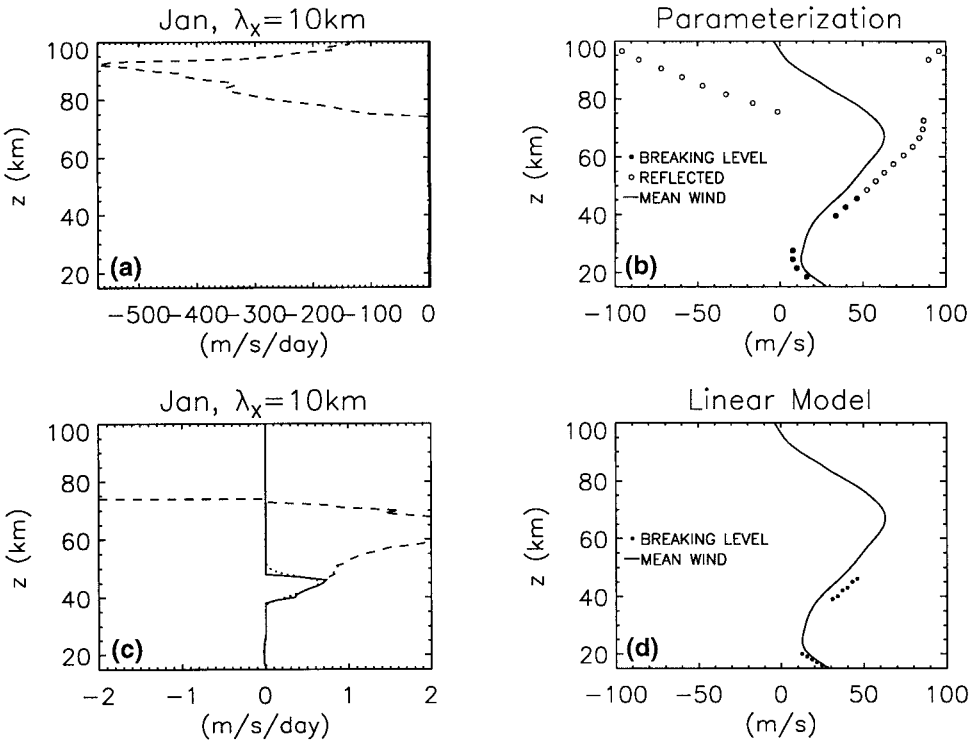

FIG. 3. Forcing, zonal wind, and breaking levels for 10-km horizontal wavelength waves. (a), (c) Profiles of parameterized gravity wave–driven zonal force neglecting reflection (dashed line), including reflection (solid), and comparison to a linear model with a saturation condition (dotted); (b) zonal wind profile for this case (solid) and breaking levels vs phase speed for the parameterization neglecting reflection (both open and filled circles) and including reflection (filled circles only); (d) same as (b) but for the linear model that includes nonhydrostatic and rotation effects.

find it necessary to include the effects of rotation and consider the shear instability mechanism for the determination of the breaking levels.

Figures 3, 4, and 5 demonstrate that waves of different horizontal scales have some fundamental differences in their interactions with the background atmosphere. In the future, if warranted, nonhydrostatic and rotation effects could be included at the cost of increased complexity in the calculations. The effects of total internal reflection will be included here, because the results in this section show that these can be substantial for horizontal wavelengths less than 50 km or for longer waves if the background wind speeds are larger than in these examples.

Figure 6 compares the force predicted by the parameterization and the linear model with saturation if the momentum flux (F_{S0}) was equipartioned between three horizontal wavelength bands at 10, 100, and 1000 km using the same January background atmosphere as well as examples from April and July. Both the parameterization and the linear model include total internal reflection. Profiles of mean-flow forcing in Fig. 6 calculated from the two methods are qualitatively similar, but the forcing obtained from the parameterization is usually shifted downward in altitude a bit, as might be expected, since the forcing due to each spectral component is concentrated at the breaking level rather than spread between the breaking level and higher altitudes. Tests with a single wavelength of 100 km have also been performed and can produce reasonable results with a factor of 3 savings in computation time; however, the parameterized forcing can then display more sudden onsets in z that may be problematic in some models.

In general, when the shear and the range of wind speeds in the background profile is small, higher phase speed resolution is required for the source spectrum input to the parameterization than when these are large. Spectral resolution should therefore be selected with weak shear profiles in mind. For maximum accuracy and computation speed, the spectral resolution would be variable depending on the total range of background wind velocity in the vertical profile, choosing (a) a wide range of phase speeds at coarse resolution when the range of wind speeds in the profile is large (strong shear) and (b) a narrower range of phase speeds at fine resolution when the range of wind speeds in the profile is small (weak shear). Courser vertical resolution in a model allows proportional decreases in the spectral resolution needed in the parameterization. For the examples shown, $\Delta c = 0.6$ m s^{-1} and $\Delta z = 1$ km. Much of the vertical structure in Fig. 6 results from the real sensi-

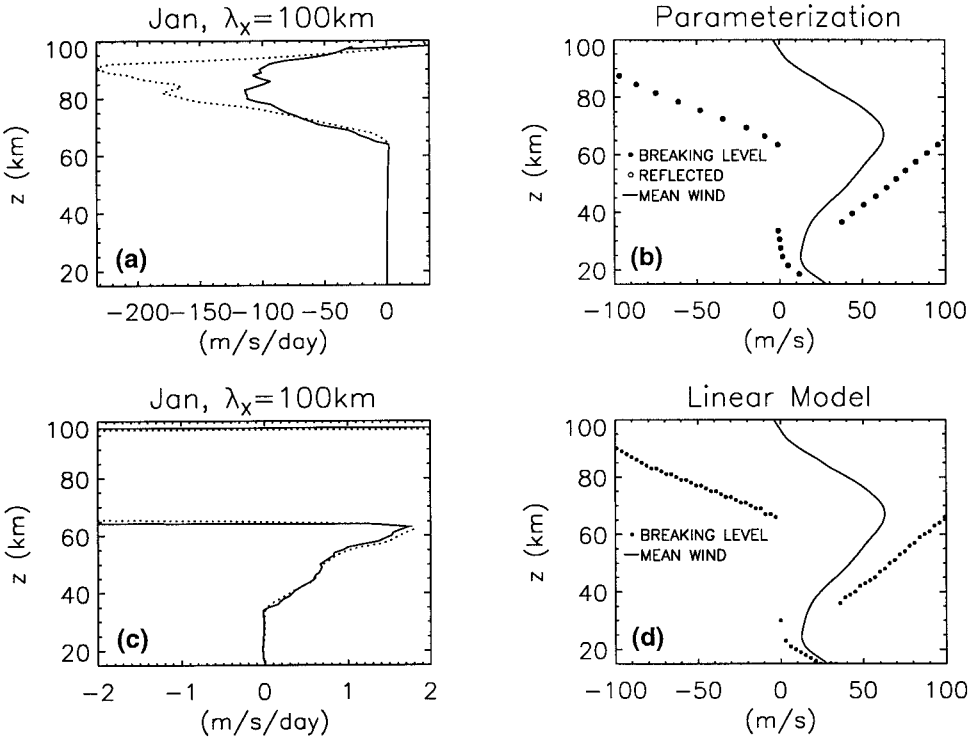

FIG. 4. Same as Fig. 3 but for waves with 100-km horizontal wavelengths.

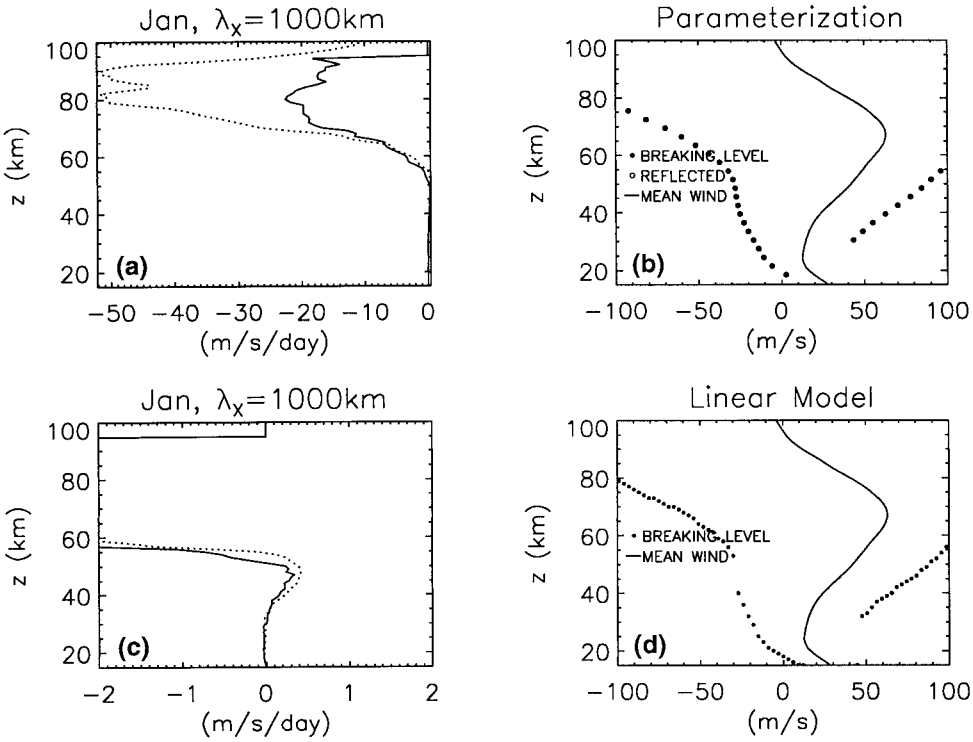

FIG. 5. Same as Fig. 3 but for waves with 1000-km horizontal wavelengths.

TABLE 1. Gravity wave source input parameters.

Source	Shape	Amplitude B_m (m^2 s^{-2})	Net flux F_{S0} (Pa)	Imput altitude (km)
Topography (Fig. 7)	Eq. (17) $c_w = 1$ m s^{-1}	1.0	0.5*	3
Broad (Fig. 8)	Eq. (17) $c_w = 60$ m s^{-1}	0.4	4×10^{-3}	15
Convection (Fig. 9)	Eq. (29) $c_p = 25$ m s^{-1}	1.2	4×10^{-3} average	15

*Local flux over mountains. The zonal mean flux is further multiplied by the fractional coverage (Fig. 7b).

tivity of the parameterization to subtle variations in wind shear and stability with height.

4. Parameterization results

In this section, we show some simple applications of the parameterization for illustration.

a. Mountain wave source

To represent topographically generated waves, a narrow spectrum peaking at $c = 0$ is input to the parameterization (Fig. 7a). This spectrum follows the common wisdom that topographic waves are approximately stationary, but allows for some nonstationary waves as well (Nance and Durran 1997; Worthington and Thomas 1998). January zone-mean wind and temperature fields from CIRA (Fleming et al. 1990) are used to specify the background atmosphere. For this zonal-mean estimate, the net gravity wave momentum flux F_{S0} input at the source level is multiplied by an additional fraction (Fig. 7b) representing a fractional coverage of topographic slopes derived from the National Center for Atmospheric Research 2.5° × 2.5° topography database. This is used to estimate the fractional area of each latitude band covered by mountains, a factor included in the intermittency that will now vary with latitude. No variations in wave amplitudes B_m are included, and only

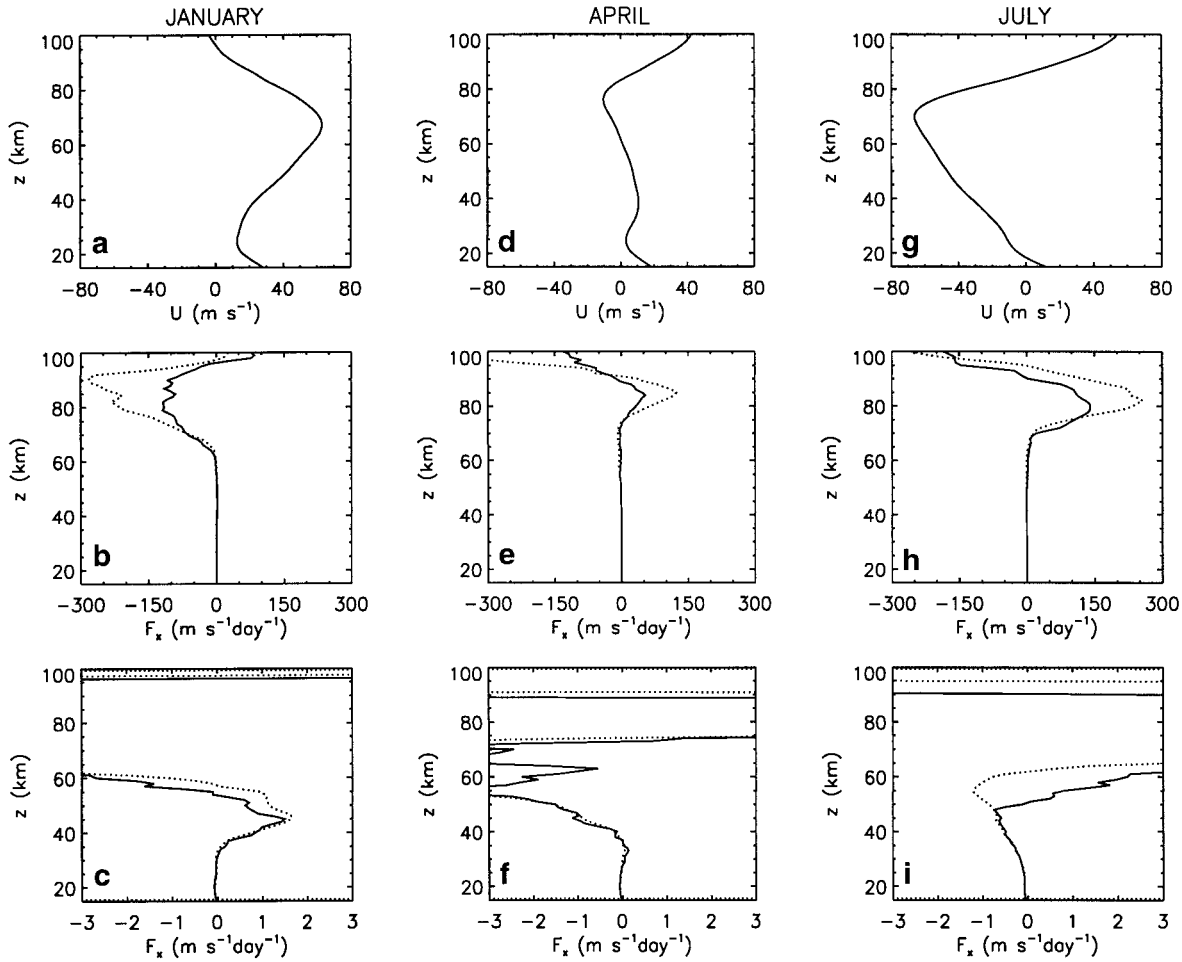

FIG. 6. Parameterization results with the background atmosphere from CIRA zonal means at 40°N lat: (a) zonal wind, Jan; (b), (c) Jan parameterized force (solid line) and the force from the linear model with saturation (dotted line); (d) zonal wind, Apr; (e), (f) Apr parameterized force (solid line) and the force from the linear model with saturation (dotted line); (g) zonal wind, Jul; (h), (i) Jul parameterized force (solid line) and the force from the linear model with saturation (dotted line).

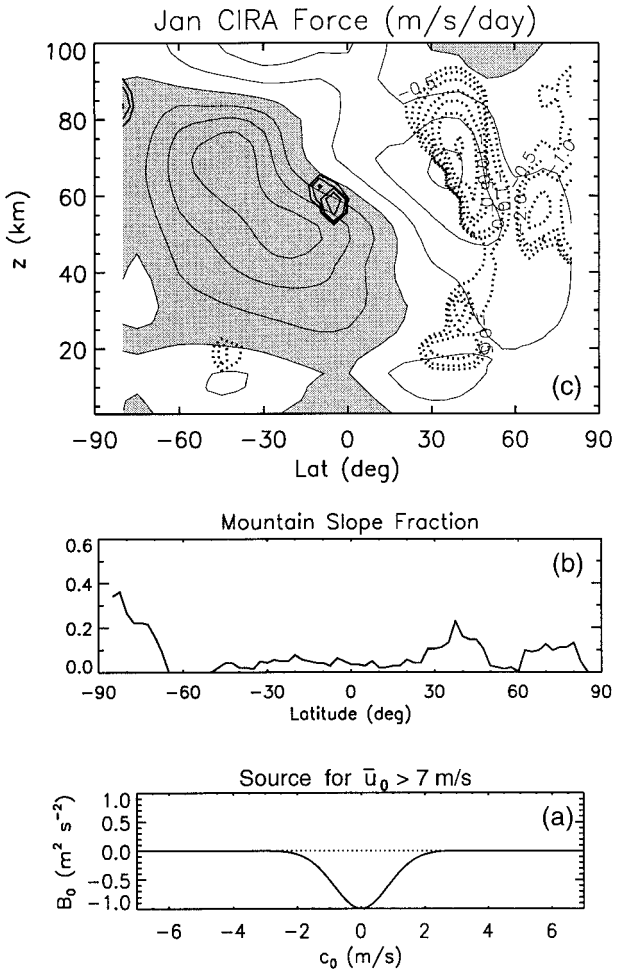

FIG. 7. An example application of the parameterization for topographic waves (see also Table 1): (a) mountain wave source momentum flux vs phase speed; (b) fractional coverage of mountain slopes vs lat; (c) parameterized zonal-mean force (thick lines) vs latitude and height. Dashed contours represent westward forcing, solid eastward. Contours are chosen at pseudologarithmic intervals: $\pm$0.5, 1, 2, 5, 10, 50 m s^{-1} day^{-1}. The thin lines show the background wind for this January case at 20 m s^{-1} intervals. Shading shows regions of westward background winds.

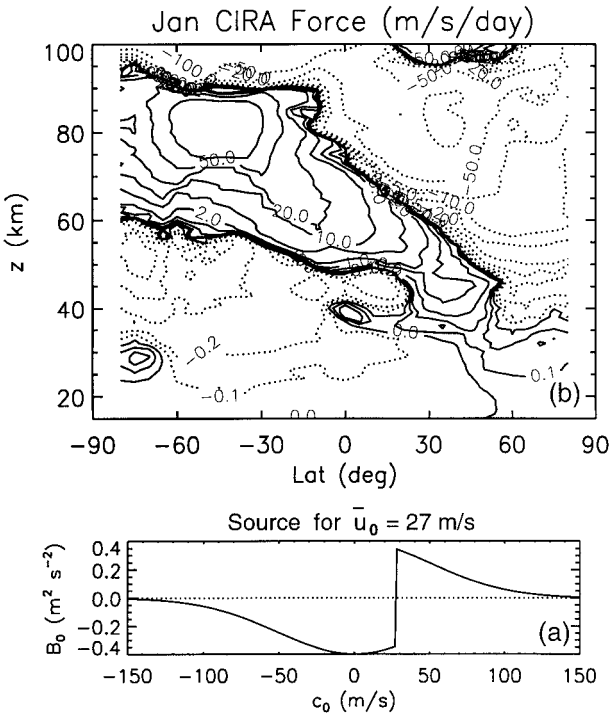

FIG. 8. Example application of the parameterization for a broad nonstationary source spectrum and Jan zonal mean winds (see also Table 1). (a) Momentum flux spectrum vs phase speed. Note that the phase speed where the flux changes sign will vary with the zonal wind $\bar{u}_0$ at each latitude. (b) Parameterized zonal mean force as a function of latitude and height. Dashed contours represent westward forcing, solid eastward. Contours are chosen at pseudologarithmic intervals: $\pm$0.5, 1, 2, 5, 10, 50 m s^{-1} day^{-1}. The zonal winds are the same as those in Fig. 7c.

zonally propagating waves are considered in this calculation. Table 1 lists the parameter values chosen. A cross section of the parameterized January zonal-mean gravity-wave-driven force for the mountain wave source is shown in Fig. 7c. With these simple assumptions and the observationally constrained input parameters, the zonal-mean force predicted is 1–2 m s^{-1} day^{-1} above the subtropical tropospheric jets, and a peak force of 50 m s^{-1} day^{-1} at 40°N appears in the winter mesosphere. In three-dimensional global models, the parameterization should be coupled to more realistic three-dimensional topographic source parameter variations such as those in Bacmeister (1993) and used to calculate the wave-driven force on the atmosphere aloft.

b. Nonstationary wave sources

Figure 8b shows the parameterized zonal-mean gravity-wave-driven force using the broad source spectrum described in Fig. 8a and Table 1. The same January CIRA background atmosphere is specified (see Fig. 7c). (Note that the CIRA standard does not include the large-amplitude QBO variations in the equatorial region. The shear associated with the QBO will substantially modify gravity wave interactions with the mean flow at the equator, so equatorial features in Fig. 8 are not likely to be very realistic.) In the extratropics, this broad source generates the drag forces needed in the mesosphere (Holton 1982; Fritts 1989) and an accelerative westward force in the summer stratosphere that may be important to the stratospheric residual circulation (Alexander and Rosenlof 1996). In these regions, gravity waves may dominate the wave-driven forcing in the atmosphere. In the winter stratosphere, planetary waves and topographic gravity waves are likely to dominate the wave-driven forcing, while the nonstationary waves that went into Fig. 8 likely play a relatively minor role. The effects of these nonstationary gravity waves on the residual circulation in the stratosphere have yet to be

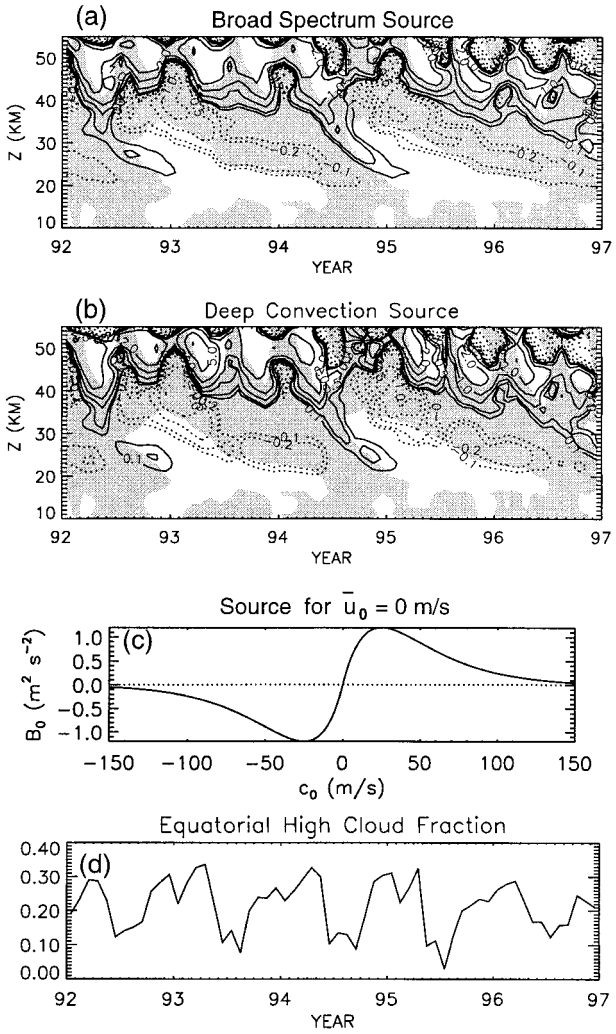

FIG. 9. Example illustrating equatorial time–height maps of forcing in the stratosphere: (a) forcing for the broad source in Table 1 and Fig. 8a with no time variations in the momentum flux; (b) forcing for the convection source in Table 1 and shown in (c). The source momentum flux varies in time according to the fractional coverage of high clouds at the equator (d), but the time-average flux input is the same as that for (a). The contours plotted in (a) and (b) are ± 0.1, 0.2, 0.5, 1, 2, 5, 10 m s^{-1} day^{-1}. Shading shows regions where the background zonal winds are westward showing the QBO and semiannual oscillation variations in the winds.

examined in global models, but such studies are in progress.

c. Tropical convectively generated gravity waves

The effects of convective gravity wave sources can be studied with the parameterization. The nature of convectively generated gravity waves is still poorly constrained by observations, but as such details become available, the parameterization should be a useful tool for studying their effects aloft. As an illustration, time–altitude cross sections of gravity-wave-driven zonal-mean force at the equator are shown in Fig. 9. The shading shows regions where the background wind is westward. The winds here were derived from the *Upper Atmosphere Research Satellite* program (see Ray et al. 1998). Figure 9a shows the parameterized gravity-wave-driven force using the broad spectrum in Fig. 8a and Table 1 input at 15-km altitude. The source spectrum changes slightly in time as the mean wind changes and moves the position of zero intrinsic phase speed ($\bar{u} - c = 0$) within the spectrum. The force in Fig. 9a is quite similar to the results shown in Ray et al. (1998) using the same background atmosphere, and similar gravity wave source characteristics input to the linear model described earlier (Alexander 1998).

For Fig. 9b, a convection-based gravity wave source was instead specified. The source spectrum is plotted in Fig. 9c for $\bar{u} = 0$ conditions. The central phase speed will shift with the winds at 15 km. This source spectrum is loosely based on the results of numerical simulations (Alexander and Holton 1997) and has the analytical form (Dunkerton 1997)

$$B_0(\hat{c}) = B_m\left(\frac{\hat{c}}{c_p}\right)\exp(1 - |\hat{c}/c_p|). \tag{29}$$

The input parameters are summarized in Table 1. The net flux in the gravity wave spectrum at 15 km is varied in time according to a fraction of areal coverage of high clouds in the 3.75°S–3.75°N latitude band (Fig. 9d) derived from the record of monthly mean 2.5° × 2.5° interpolated outgoing longwave radiation (OLR < 215 W m^{-2}). Let χ_c represent this fraction. The net flux input at 15 km at each time into the parameterization is

$$F_{s0}(t) = \chi_c \frac{(4 \times 10^{-3}\text{Pa})}{\overline{\chi_c}^t}, \tag{30}$$

where $\overline{(\chi_c)}^t$ is the time-averaged fraction. The 5-yr average flux input is then the same in both Figs. 9a and 9b, the convection source in Fig. 9b is seasonally variable, so the net flux and wave intermittency vary in time.

Comparing Figs. 9a and 9b, the two results are qualitatively very similar. Quasi-biennial and semiannual oscillations in forcing appear in both with similar magnitudes. The QBO forcing in particular is not very sensitive to the shape of the spectrum, but only to the total flux in the spectrum carried by waves with the range of phase speeds equal to the range of wind speeds (Dunkerton 1997). The primary difference in the convection case is an enhancement in the semiannual variability in the upper stratosphere caused by the time variations in χ_c. These forcing estimates have not yet been tested in models, so no conclusions can be drawn here about the effects of the parameterized estimates. The parameterization should be well suited to studying, predicting, and analyzing the effects of different details of gravity wave sources that we can learn from future observations.

5. Discussion

The parameterized gravity-wave-driven forcing estimates presented here were restricted to single vertical profiles or zonal means. The parameterization is meant to apply to three-dimensional global models as well. This can be accomplished by simple application of the parameterization as a one-dimensional calculation using wind and stability profiles at each geographic point in the model. Studying the interactions between gravity waves and planetary-scale waves, including tides, will be a natural extension and can be accomplished by treating the sum of the mean plus large-scale wave perturbations as the background atmosphere through which the waves propagate. The appropriateness of such an approach should be considered carefully, however. The parameterization relies on linear theory to describe the wave propagation. By definition, the ''background'' atmosphere is slowly varying in space and time compared to the scales of the wave propagation and dissipation. Group velocities of the members of the gravity wave spectrum can vary widely across the spectrum and will vary for each member of the spectrum with height. The underlying assumption in including large-scale waves in the background is that those larger waves vary slowly over the interaction time interval with the waves. Eckermann (1997) suggests that this may be a poor assumption in some cases. In the stratosphere, waves tend to break at altitudes where their group velocities may be quite slow, so the approximation will be more questionable there. In the mesosphere, group velocities of breaking waves tend to be much larger. The parameterization assumes that waves propagate only vertically from their sources in the lower atmosphere. For ray paths to be truly vertical, fast vertical group propagation would be required, and wave refraction would have to be negligible [see Dunkerton (1984) for illustration]. These assumptions could become inappropriate for gravity waves propagating through larger-scale waves treated as the background wind (Eckermann and Marks 1996).

Global models will likely continue to improve their horizontal resolutions in the future. At high resolution, the application of unique vertical profiles of the force at each geographic point may become inappropriate, in part because of the horizontal dispersion of the waves as they propagate from the troposphere vertically, but also in part due to nonlinear effects. In nonlinear simulations that resolve gravity wave breaking (Durran 1995), it has been shown that, although momentum dissipation may be very localized in the horizontal, the mean-flow response occurs over much larger areas on very short timescales. Apparently the momentum in the wave–mean-flow interaction in Durran's (1995) simulation is transported horizontally by very high-speed gravity waves and/or infrasound waves away from the primary wave-breaking region. Zhu and Holton (1987) studied emission of low-frequency waves through geostrophic adjustment in the region of localized forcing, a process that would also delocalize the mean-flow effects. It may be necessary in future higher-resolution GCMs to apply a horizontal smoothing function to the force to approximate these effects before applying it in the momentum equation. We may, in fact, have already reached these limits in the application of spatially varying topographic gravity wave drag in some higher-resolution global models. Klinker and Sardeshmukh (1992) have shown that initial tendency errors in the European Centre for Medium-Range Weather Forecasts assimilation are closely tied to the geographic patterns in gravity wave drag.

The parameterization assumes that waves propagate without dissipation until breaking occurs. This assumption will certainly be violated above the homopause where molecular diffusion becomes important. To apply this parameterization above 100-km altitude, some kind of dissipation should be applied across the parameterized gravity wave spectrum to account for the effects of molecular diffusion at those altitudes (Pitteway and Hines 1963).

Acknowledgments. This research was supported by National Science Foundation Grants ATM-9896269 and ATM-9500613, and by National Aeronautics and Space Administration Contract NAS1-96071.

REFERENCES

Alexander, M. J., 1996: A simulated spectrum of convectively generated gravity waves: Propagation from the tropopause to the mesopause and effects on the middle atmosphere. *J. Geophys. Res.,* **101,** 1571–1588.

——, 1998: Interpretations of observed climatological patterns in stratospheric gravity wave variance. *J. Geophys. Res.,* **103,** 8627–8640.

——, and L. Pfister, 1995: Gravity wave momentum flux in the lower stratosphere over convection. *Geophys. Res. Lett.,* **22,** 2029–2032.

——, and K. H. Rosenlof, 1996: Nonstationary gravity wave forcing of the stratospheric zonal mean wind. *J. Geophys. Res.,* **101,** 23 465–23 474.

——, and J. R. Holton, 1997: A model study of zonal forcing in the equatorial stratosphere by convectively induced gravity waves. *J. Atmos. Sci.,* **54,** 408–419.

Andreassen, O., C. E. Wasberg, D. C. Fritts, and J. R. Isler, 1994: Gravity wave breaking in two and three dimensions, 1. Model description and comparison of two-dimensional evolutions. *J. Geophys. Res.,* **99,** 8095–8108.

Andrews, D. G., J. R. Holton, and C. B. Leovy, 1987: *Middle Atmosphere Dynamics.* Academic Press, 489 pp.

Bacmeister, J. T., 1993: Mountain-wave drag in the stratosphere and mesosphere inferred from observed winds and a simple mountain-wave parameterization scheme. *J. Atmos. Sci.,* **50,** 377–399.

Broutman, D., C. Macaskill, M. E. McIntyre, and J. W. Rottmann, 1997: On Doppler-spreading models of internal waves. *Geophys. Res. Lett.,* **24,** 2813–2816.

Chang, J. L., S. K. Avery, A. C. Riddle, S. E. Palo, and K. S. Gage, 1997: First results of tropospheric gravity wave momentum flux measurements over Christmas Island. *Radio Sci.,* **32,** 727–748.

Coy, L., and D. C. Fritts, 1988: Gravity wave heat fluxes: A Lagrangian approach. *J. Atmos. Sci.,* **45,** 1770–1780.

Dewan, E. M., and R. E. Good, 1986: Saturation and the ''universal''

spectrum for vertical profiles of horizontal scalar winds in the atmosphere. *J. Geophys. Res.,* **91,** 2742–2748.
——, and Coauthors, 1998: MSX satellite observations of thunderstorm-generated gravity waves in mid-wave infrared images of the upper stratosphere. *Geophys. Res. Lett.,* **25,** 939–942.
Dunkerton, T. J., 1984: Inertia–gravity waves in the stratosphere. *J. Atmos. Sci.,* **41,** 3396–3404.
——, 1989: Theory of internal gravity wave saturation. *Pure Appl. Geophys.,* **130,** 373–397.
——, 1997: The role of gravity waves in the quasi-biennial oscillation. *J. Geophys. Res.,* **102,** 26 053–26 076.
Durran, D. D., 1995: Do breaking mountain waves decelerate the local mean flow? *J. Atmos. Sci.,* **52,** 4010–4032.
Eckermann, S. D., 1997: Influence of wave propagation on the Doppler spreading of atmospheric gravity waves. *J. Atmos. Sci.,* **54,** 2554–2573.
——, and C. J. Marks, 1996: An idealized ray model of gravity wave-tidal interactions. *J. Geophys. Res.,* **101,** 21 195–21 212.
Fleming, E. L., S. Chandra, J. J. Barnett, and M. Corney, 1990: Zonal mean temperature, pressure, zonal wind and geopotential height as functions of latitude. *Adv. Space Res.,* **10** (12), 11–59.
Fritts, D. C., 1984: Gravity wave saturation in the middle atmosphere: A review of theory and observations. *Rev. Geophys. Space Phys.,* **22,** 275–308.
——, 1989: A review of gravity wave saturation processes, effects, and variability in the middle atmosphere. *Pure Appl. Geophys.,* **130,** 343–371.
——, and T. J. Dunkerton, 1985: Fluxes of heat and constituents due to convectively unstable gravity waves. *J. Atmos. Sci.,* **42,** 549–556.
——, and R. A. Vincent, 1987: Mesospheric momentum flux studies at Adelaide, Australia: Observations and a gravity wave–tidal interaction model. *J. Atmos. Sci.,* **44,** 605–619.
——, and W. Lu, 1993: Spectral estimates of gravity wave energy and momentum fluxes. Part II: Parameterization of wave forcing and variability. *J. Atmos. Sci.,* **50,** 3695–3713.
——, and T. E. VanZandt, 1993: Spectral estimates of gravity wave energy and momentum fluxes. Part I: Energy dissipation, acceleration, and constraints. *J. Atmos. Sci.,* **50,** 3685–3694.
——, T. Tsuda, T. E. VanZandt, S. A. Smith, T. Sato, S. Fukao, and S. Kato, 1990: Studies of velocity fluctuations in the lower atmosphere using the MU radar. Part II: Momentum fluxes and energy densities. *J. Atmos. Sci.,* **47,** 51–66.
——, J. R. Isler, and Ø. Andreassen, 1994: Gravity wave breaking in two and three dimensions, 2: Three-dimensional evolution and instability structure. *J. Geophys. Res.,* **99,** 8109–8124.
Garcia, R. R., and S. Solomon, 1985: The effect of breaking gravity waves on the dynamics and chemical composition of the mesosphere and lower thermosphere. *J. Geophys. Res.,* **90,** 3850–3868.
Hines, C. O., 1991: The saturation of gravity waves in the middle atmosphere. Part I: Critique of linear-instability theory. *J. Atmos. Sci.,* **48,** 1348–1359.
——, 1997: Doppler-spread parameterization of gravity-wave momentum deposition in the middle atmosphere. 1. Basic formulation. *J. Atmos. Sol.-Terr. Phys.,* **59,** 371–86.
Holton, J. R., 1982: The role of gravity wave induced drag and diffusion in the momentum budget of the mesosphere. *J. Atmos. Sci.,* **39,** 791–799.
——, and R. S. Lindzen, 1972: An updated theory for the quasi-biennial cycle of the tropical stratosphere. *J. Atmos. Sci.,* **29,** 1076–1080.
Jackson, D. R., and L. J. Gray, 1994: Simulation of the semi-annual oscillation of the equatorial middle atmosphere using the Extended UGAMP General Circulation Model. *Quart. J. Roy. Meteor. Soc.,* **120,** 1559–1588.
Kiehl, J. T., J. J. Hack, G. B. Bonan, B. A. Boville, B. P. Briegleb, D. L. Williamson, and P. J. Rasch, 1996: Description of the NCAR Community Climate Model (CCM3). NCAR Tech. Note 420, 152 pp. [Available from NCAR, P.O. Box 3000, Boulder, CO 80307-3000.]
Klinker, E., and P. D. Sardeshmukh, 1992: The diagnosis of mechanical dissipation in the atmosphere from large-scale balance requirements. *J. Atmos. Sci.,* **49,** 608–627.
Lelong, M.-P., and T. J. Dunkerton, 1998a: Inertia–gravity wave breaking in three dimensions. Part I: Convectively stable waves. *J. Atmos. Sci.,* **55,** 2473–2488.
——, and ——, 1998b: Inertia–gravity wave breaking in three dimensions. Part II: Convectively unstable waves. *J. Atmos. Sci.,* **55,** 2489–2501.
Lighthill, J., 1978: *Waves in Fluids*. Cambridge University Press, 504 pp.
Lindzen, R. S., 1981: Turbulence and stress owing to gravity wave and tidal breakdown. *J. Geophys. Res.,* **86,** 9707–9714.
——, 1985: Multiple gravity-wave breaking levels. *J. Atmos. Sci.,* **42,** 301–305.
——, and J. R. Holton, 1968: A theory of the quasi-biennial oscillation. *J. Atmos. Sci.,* **25,** 1095–1107.
Marks, C. J., and S. D. Eckermann, 1995: A three-dimensional nonhydrostatic ray-tracing model for gravity waves: Formulation and preliminary results for the middle atmosphere. *J. Atmos. Sci.,* **52,** 1959–1984.
McFarlane, N. A., 1987: The effect of orographically excited gravity wave drag on the general circulation of the lower stratosphere and troposphere. *J. Atmos. Sci.,* **44,** 1775–1800.
McIntyre, M. E., 1989: On dynamics and transport near the polar mesopause in summer. *J. Geophys. Res.,* **94,** 14 617–14 628.
Medvedev, A. S., and G. P. Klaassen, 1995: Vertical evolution of gravity wave spectra and the parameterization of associated wave drag. *J. Geophys. Res.,* **100,** 25 841–25 853.
Murayama, Y., T. Tsuda, and S. Fukao, 1994: Seasonal variation of gravity wave activity in the lower atmosphere observed with the MU radar. *J. Geophys. Res.,* **99,** 23 057–23 069.
Nance, L. B., and D. R. Durran, 1997: A modeling study of nonstationary trapped mountain lee waves. Part I: Mean flow variability. *J. Atmos. Sci.,* **54,** 2275–2291.
Norton, W. A., and J. Thuburn, 1996: The two-day wave in a middle atmosphere 6CM. *Geophys. Res. Lett.,* **23,** 2113–2116.
O'Sullivan, D., and T. J. Dunkerton, 1995: Generation of inertia-gravity waves in a simulated life cycle of baroclinic instability. *J. Atmos. Sci.,* **52,** 3695–3716.
Palmer, T. N., G. J. Shutts, and R. Swinbank, 1986: Alleviation of a systematic westerly bias in general circulation and numerical weather prediction models through an orographic gravity wave drag parameterization. *Quart. J. Roy. Meteor. Soc.,* **112,** 1001–1039.
Pfister, L., and Coauthors, 1993: Gravity waves generated by a tropical cyclone during the STEP tropical field program: A case study. *J. Geophys. Res.,* **98,** 8611–8638.
Pitteway, M. L. V., and C. O. Hines, 1963: The viscous damping of atmospheric gravity waves. *Can. J. Phys.,* **41,** 1935–1948.
Prichard, I. T., and L. Thomas, 1993: Radar observations of gravity-wave momentum fluxes in the troposphere and lower stratosphere. *Ann. Geophys.,* **11,** 1075–1083.
——, ——, and R. M. Worthington, 1995: The characteristics of mountain waves observed by radar near the west coast of Wales. *Ann. Geophys.,* **13,** 757–767.
Prusa, J., P. K. Smolarkiewicz, and R. R. Garcia, 1996: Propagation and breaking at high altitudes of gravity waves excited by tropospheric forcing. *J. Atmos. Sci.,* **53,** 2186–2216.
Ray, E. A., M. J. Alexander, and J. R. Holton, 1998: An analysis of the structure and forcing of the equatorial semiannual oscillation in zonal wind. *J. Geophys. Res.,* **103,** 1759–1774.
Reeder, M. J., and M. Griffiths, 1996: Stratospheric inertia-gravity waves generated in a numerical model of frontogenesis. II: Wave sources and generation mechanisms. *Quart. J. Roy. Meteor. Soc.,* **122,** 1175–1195.
Rind, D., R. Suozzo, and N. K. Balachandran, 1988: The GISS global climate–middle atmosphere model. Part II: Model variability due

to interactions between planetary waves, the mean circulation and gravity wave drag. *J. Atmos. Sci.,* **45,** 371–386.
Sato, K., 1990: Vertical wind disturbances in the troposphere and lower stratosphere observed by the MU radar. *J. Atmos. Sci.,* **47,** 2803–2817.
——, 1992: Vertical wind disturbances in the afternoon of mid-summer revealed by the MU radar. *Geophys. Res. Lett.,* **19,** 1943–1946.
——, 1993: Small-scale wind disturbances observed by the MU radar during the passage of Typhoon Kelly. *J. Atmos. Sci.,* **50,** 518–537.
——, 1994: A statistical study of the structure, saturation and sources of inertio-gravity waves in the lower stratosphere observed with the MU radar. *J. Atmos. Terr. Phys.,* **56,** 755–774.
——, and M. Yamada, 1994: Vertical structure of atmospheric gravity waves revealed by the wavelet analysis. *J. Geophys. Res.,* **99,** 20 623– 20 631.
——, and T. J. Dunkerton, 1997: Estimates of momentum flux associated with equatorial Kelvin and gravity waves. *J. Geophys. Res.,* **102,** 26 247–26 261.
——, F. Hasegawa, and I. Hirota, 1994: Short-period disturbances in the equatorial lower stratosphere. *J. Meteor. Soc. Japan,* **72,** 859–872.
——, D. O'Sullivan, and T. J. Dunkerton, 1997: Low-frequency inertia-gravity waves in the stratosphere revealed by three-week continuous observation with the MU radar. *Geophys. Res. Lett.,* **24,** 1739–1742.
Smith, S. A., D. C. Fritts, and T. E. VanZandt, 1987: Evidence for a saturated spectrum of atmospheric gravity waves. *J. Atmos. Sci.,* **44,** 1404–1410.
Swenson, G. R., and P. J. Espy, 1995: Observations of two-dimensional airglow structure and Na density from the ALOHA, October 9, 1993, ''Storm Flight.'' *Geophys. Res. Lett.,* **22,** 2845–2848.
Taylor, M. J., Y. Y. Gu, X. Tao, C. S. Gardner, and M. B. Bishop, 1995: An investigation of intrinsic gravity wave signatures using coordinated lidar and nightglow image measurements. *Geophys. Res. Lett.,* **22,** 2853–2856.
Warner, C. D., and M. E. McIntyre, 1996: On the propagation and dissipation of gravity wave spectra through a realistic middle atmosphere. *J. Atmos. Sci.,* **53,** 3213–3235.
Worthington, R. M., and L. Thomas, 1998: The frequency spectrum of mountain waves. *Quart. J. Roy. Meteor. Soc.,* **124,** 687–703.
Zhu, X., 1994: A new theory of the saturated gravity wave spectrum for the middle atmosphere. *J. Atmos. Sci.,* **51,** 3615–3626.
——, and J. R. Holton, 1987: Mean fields induced by local gravity-wave forcing in the middle atmosphere. *J. Atmos. Sci.,* **44,** 620–630.